ADVANCED MATERIALS
www.advmat.de

Scalable Fabrication of Molybdenum Disulfide Nanostructures and their Assembly

*Yun Huang, Kang Yu, Huaizhi Li, Kai Xu, Zexi Liang, Debora Walker, Paulo Ferreira, Peer Fischer, and Donglei (Emma) Fan**

Molybdenum disulfide (MoS_2) is a multifunctional material that can be used for various applications. In the single-crystalline form, MoS_2 shows superior electronic properties. It is also an exceptionally useful nanomaterial in its polycrystalline form with applications in catalysis, energy storage, water treatment, and gas sensing. Here, the scalable fabrication of longitudinal MoS_2 nanostructures, i.e., nanoribbons, and their oxide hybrids with tunable dimensions in a rational and well-reproducible fashion, is reported. The nanoribbons, obtained at different reaction stages, that is, MoO_3, MoS_2/MoO_2 hybrid, and MoS_2, are fully characterized. The growth method presented herein has a high yield and is particularly robust. The MoS_2 nanoribbons can readily be removed from its substrate and dispersed in solution. It is shown that functionalized MoS_2 nanoribbons can be manipulated in solution and assembled in controlled patterns and directly on microelectrodes with UV-click-chemistry. Owing to the high chemical purity and polycrystalline nature, the MoS_2 nanostructures demonstrate rapid optoelectronic response to wavelengths from 450 to 750 nm, and successfully remove mercury contaminants from water. The scalable fabrication and manipulation followed by light-directed assembly of MoS_2 nanoribbons, and their unique properties, will be inspiring for device fabrication and applications of the transition metal dichalcogenides.

Transition metal dichalcogenides (TMD) have attracted immense research interest owing to their 2D stacking molecular structures and the resulted chemical and physical properties.[1] Among various TMD materials, single-crystal molybdenum disulfide (MoS_2) nanoflakes in the 2H-phase, which constitute the basic unit of various crystalline MoS_2 nanostructures and bulk MoS_2, possess edge sites and in plane sulfur vacancies which for instance show outstanding catalytic activity with an ultralow hydrogen adsorption Gibbs free energy—similar to that of the most efficient platinum and other noble metals.[2] However, in contrast to platinum, MoS_2 is much cheaper, and because it is a semiconductor, its electric conductivity can be readily tuned by the application of a voltage or light. This has been exploited in a variety of applications. For instance, MoS_2 has been demonstrated as an optical and biochemical sensor material.[3] MoS_2 field-effect transistors exhibit an on/off ratio as high as $\approx 10^8$ and near-ideal subthreshold

Y. Huang, Dr. K. Yu, H. Li, Z. Liang, Prof. P. Ferreira, Prof. D. Fan
Materials Science and Engineering Program
Texas Materials Institute
The University of Texas at Austin
Austin, TX 78712, USA
E-mail: dfan@austin.utexas.edu
Dr. K. Yu, Prof. P. Ferreira
The Department of Advanced Electron Microscopy
Imaging and Spectroscopy
International Iberian Nanotechnology Laboratory
Braga 4715-330, Portugal
Dr. K. Xu
Electrical and Computer Engineering
University of Illinois at Urbana-Champaign
Urbana, IL 61801, USA
Dr. D. Walker
School of Engineering and Applied Sciences
Harvard University
Cambridge, MA 02138, USA
The ORCID identification number(s) for the author(s) of this article can be found under https://doi.org/10.1002/adma.202003439.
Prof. P. Ferreira
Mechanical Engineering Department and IDMEC
Instituto Superior Técnico
University of Lisbon
Av. Rovisco Pais, Lisboa 1049-001, Portugal
Prof. P. Fischer
Max-Planck-Institute for Intelligent Systems
Heisenbergstr. 3, Stuttgart 70569, Germany
Prof. P. Fischer
Institute of Physical Chemistry
University of Stuttgart
Pfaffenwaldring 55, Stuttgart 70569, Germany
Prof. D. Fan
Walker Department of Mechanical Engineering
The University of Texas at Austin
Austin, TX 78712, USA

DOI: 10.1002/adma.202003439

swing of ≈65 mV dec^{-1}.[4] Flakes of MoS_2 have been used for water treatment for the removal of mercury.[5] Moreover, size-dependent effects, have been found when modulating dimensions of MoS_2 nanostructures.[6,7] Indeed, MoS_2 emerges as a highly promising material that may impact many research fields, including electronics,[8] catalysis,[9] energy storage,[10] water treatment,[11] and gas sensing.[12]

To realize the full potential of MoS_2, the first task is to find a convenient and robust means to scalably fabricate MoS_2 with controllable dimensions. So far, various attempts have been made to synthesize MoS_2 thin films and 3D composites via chemical vapor deposition (CVD) and hydrothermal growth.[13] Tubular MoS_2 or core–shell MoS_2/oxide nanostructures can be grown via a catalyzed transport reaction,[14] sintering of $(NH_4)_2MoS_4$ in hydrogen/thiophene,[15] and sulfurization of oxide nanobelts.[16] Nevertheless, only modest dimensional control can be realized, and the quality is variable. It remains extremely challenging to synthesize MoS_2 with a tunable geometry in larger volumes, which is imperative for applications and rational device integration. Only in a very recent report has it been shown that the dimensionality of thin MoS_2 nanoribbons could be tuned when it is grown on phosphine pre-treated Si(001) surfaces.[7] The nanoribbons are fabricated with a yield of 75%, mixed with triangle nanosheets, and they exhibited optical properties that depended on their dimensionality. The as-obtained MoS_2 nanoribbons are attached to the substrate in random positions and orientations. There is thus a notable technological gap between the unique properties of MoS_2 and its applications due to the daunting task of fabricating MoS_2 nanostructures of controlled and tunable dimensions with high yield, scalability and reproducibility.

Besides the demand in the fabrication of controlled MoS_2 nanostructures, it is of great interest to be able to assemble them into different configurations for device characterization and integration. In reality, the majority of the state-of-the-art MoS_2 nanodevices still rely on lithographic patterning of flakes of MoS_2 that are exfoliated from bulk materials or grown via CVD.[17] The device making process and assembly thus far is tedious due to the random dispersion of MoS_2 flakes, and the required efforts in removing them from a substrate.

Here, we present a robust method of growing freely dispersible MoS_2 nanostructures with tunable elongated morphologies, that is, nanoribbons, in relatively large quantities. Given the well-defined geometry of the MoS_2 nanostructures, we are able to demonstrate their assembly into various designed configurations by utilizing a combined nanomanipulation and UV-click chemical reaction. Further tests show the rapid optoelectronic response of the nanoribbons and their effectiveness in the removal of mercury from water.

The fabrication of the MoS_2 nanoribbons starts from the synthesis of MoO_3 nanoribbon precursors via a hydrothermal reaction (**Figure 1**a–c). The growth method of the MoO_3 nanoribbons is herein modified from the previously reported procedure such that large quantities can be obtained much more readily.[18] In brief, a solution containing ammonium heptamolybdate tetrahydrate and nitric acid is heated and kept at 180 °C for 20 h (Experimental Details in Supporting Information). After cooling and washing, the procedure yields a white powder of MoO_3 nanoribbons, which can be collected and dried (Figure 1a–d). The length distribution is shown in Figure S1, Supporting Information. The MoO_3 powder is placed in a two-zone furnace (Mellen TC12) at 500 °C, 25 cm from the opening inside a quartz tube sealed at one end (30 cm long and 18 mm in diameter) for 30 min, and 20 cm away from the sulfur powder inside an identical tube at 200 °C. A flow of argon gas at 50 sccm is introduced to carry the sulfur vapor such that it can react with the MoO_3 nanoribbons. The reaction produces MoS_2/MoO_2 hybrid nanoribbons (Figure 1b–e). Here, the temperature of 500 °C is carefully chosen so that the sulfurization can proceed efficiently without changing the nanoribbon morphology. We found that at a temperature of 650 °C and higher, the MoO_3 nanoribbons collapse to chains of nanoparticles (Figure S2, Supporting Information), which is perhaps not surprising as the melting temperature of bulk MoO_3 is 795 °C.[19] The conversion of MoO_3 into MoS_2/MoO_2 hybrid nanoribbons substantially increases the temperature stability, since the melting temperatures of MoS_2 and MoO_2 are as high as 2375 and 1100 °C, respectively. Finally, a second sulfurization process is carried out at 900 °C, which completely converts all hybrid MoS_2/MoO_2 nanoribbons to MoS_2 nanoribbons in 30 min (Figure 1c–f). The process is carefully designed and has been reported for the first time to the best of our knowledge. We obtain a spatula full of MoS_2 nanoribbons from one synthesis (Figure 1f inset). However, the procedure can readily be scaled up to obtain even larger quantities.

With the above fabrication process, MoO_3, hybrid MoS_2/MoO_2, and MoS_2 all form longitudinal nanostructures (Figure 1d–f). Atomic force microscopy analysis shows that these products are ribbon-like with notably different widths and thicknesses in their cross-sections (Figure S3a, Supporting Information). The chemistry and structures of the as-fabricated nanoribbons of MoO_3 (Figure 1g–j), MoS_2/MoO_2 (Figure 1h–k), and MoS_2 (Figure 1i–l) are determined by Raman spectroscopy and X-ray diffractometry (XRD). Note that the MoO_3 nanoribbons serve as both fabrication guiding templates and as the reaction source, which allows us to grow MoS_2 and MoS_2/MoO_2 nanoribbons with tunable dimensions by adjusting the dimensions of the MoO_3 precursors.

Phase-contrast transmission electron microscopy (TEM), reveals that the obtained MoO_3 nanoribbons are single crystals with an anisotropic orthorhombic layered structure (Figures S4 and S5, Supporting Information), which is consistent with a previous study.[20] The ribbons grow along the [001] and [100] orientations along their length and width, respectively. Since the reaction energy depends on the acidity of the suspension, and is distinct along different crystalline orientations, we systematically increase the acidity of the reaction suspension to tune the growth anisotropy (with pH values ranging from 0.0 to −1.0). Indeed, it is found that the growth of the MoO_3 nanoribbons along the [001] direction can be dramatically increased compared to that along the width ([100] direction), which permits the dimensions to be tuned. As shown in **Figure 2**, the length of MoO_3 crystal structures can change from a few micrometers (Figure 2a,b) to 70 μm (Figure 2e,f). The distribution can be easily refined by a simple one-step filtration. As shown in Figure 2g,h and Figure S6, Supporting Information, long (>20 μm) and short (<20 μm) ribbons synthesized as per the condition of Figure 2e can be easily separated by using a 40 μm filtration paper. For the longest ribbons, the width and thickness are around 1.2 μm and 64 nm, respectively (at pH = −1.0, Figure S3b, Supporting Information). As a result, the MoS_2 nanoribbons with lengths of up to tens of micrometers, for example, 35 μm, can be obtained

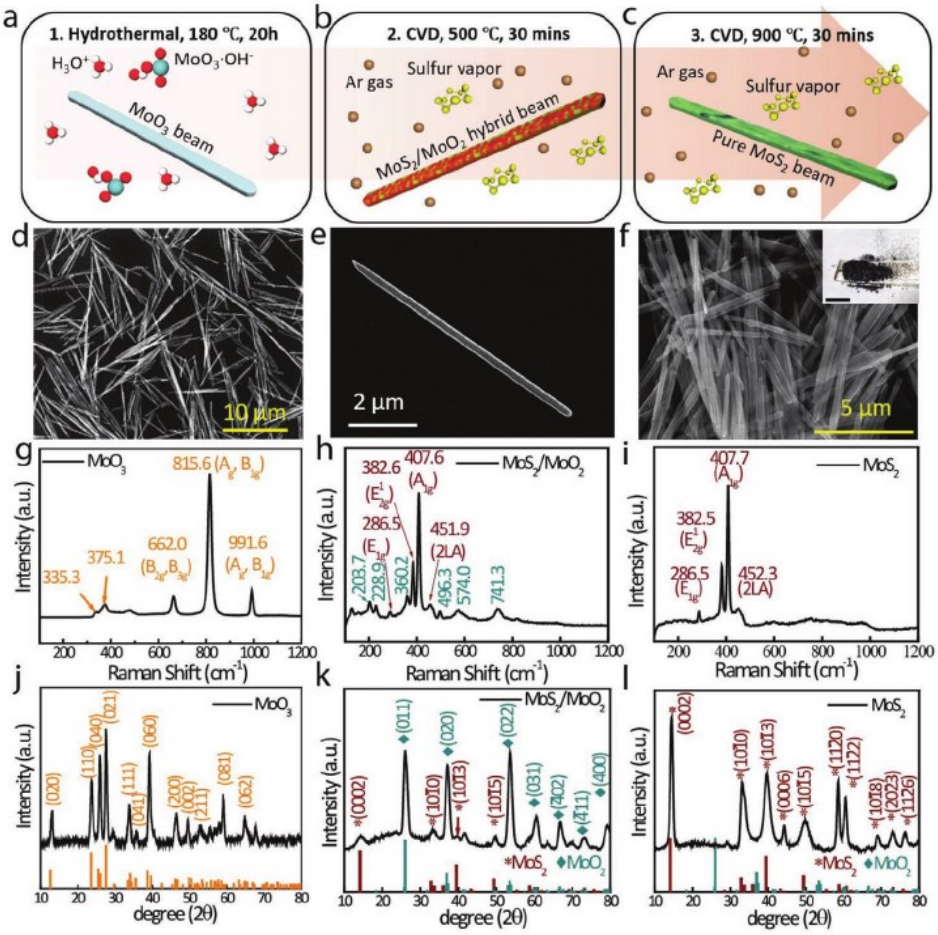

Figure 1. a–c) Schematic of the fabrication process to obtain MoS_2 nanoribbons in high yield from MoO_3 nanoribbon precursors (a), via a two-step CVD process: b) reaction to generate hybrid MoS_2/MoS_2 nanoribbons and c) conversion to MoS_2 nanoribbons. d–f) Scanning electron microscopy (SEM) images of the obtained MoO_3, MoS_2/MoO_2 hybrid and MoS_2 nanoribbons. Inset in (f): MoS_2 nanoribbons synthesized in one batch; scale bar: 1 cm. g–i) Raman and j–l) XRD spectra of MoO_3, MoS_2/MoO_2 hybrid and MoS_2 nanoribbons, respectively.

with the tunable MoO_3 as the guiding templates (Figure 2i). The corresponding Raman and XRD spectra of the long MoS_2 nanoribbons are plotted in Figure 2j–k, respectively.

Next, we examine the transition process from MoO_3 to MoS_2 in the nanoribbons by controlling the sulfurization time. At the sulfurization temperature of 500 °C, we find that the conversion of MoO_3 to the MoS_2/MoO_2 hybrid occurs as early as in the first 2 min, when strong Raman and XRD spectra of MoO_2 can be observed, and the MoO_3 signals disappear (Note S1 and Figure S7, Supporting Information). After reacting for 5 min, the Raman signals of MoS_2 and MoO_2 are observed, while the XRD signals of MoS_2 remain indistinguishable. This suggests that MoS_2 starts the growth from the surface of the nanoribbons as early as in the first 2 min while it takes between 5 and 30 min to reach a sufficient amount distinguishable by XRD (conventional XRD does not detect low-content elements, e.g., <1%).[21] After completing the 30 min sulfurization step, the Raman and XRD spectra present signals from both MoO_2 (in blue) and MoS_2 (in red) as shown in Figure 1h–k.[22] Next, with a second sulfurization at 900 °C for 30 min, only the peaks from the MoS_2 remain (Figure 1i–l). Here, in addition to supporting the Raman results, the XRD spectra (Figure 1j–l) indicate the crystalline nature of all the obtained nanoribbons.

As physical and chemical properties of these materials are closely correlated with their microstructures, it is highly desirable to examine the structures and distribution of elements of the nanoribbons, especially knowing that MoS_2 and MoO_2 exhibit distinct electronic properties. For instance, MoS_2 in the 2H-phase is a layered semiconductor with a bandgap varying from 1.2 to 1.8 eV as the thickness decreases.[6] Meanwhile, MoO_2 is known as a metallic oxide, and has been applied as electrode material in supercapacitors,[23] lithium-ion batteries,[24] and has been used for water splitting.[25] The mixture of metallic MoO_2 and layered MoS_2 could be potentially interesting for various electronic and energy storage devices. Phase-contrast TEM images from the edge and center of MoS_2/MoO_2 hybrid ribbons both reveal the (0002) MoS_2 planes with a distance of ≈0.626 nm (**Figure 3**a,b). After analyzing many TEM images of the MoS_2/MoO_2 nanoribbons (more provided in Figure S8, Supporting Information), it is found that the (0002) MoS_2 planes dominate the edges of the nanoribbons with (011) MoO_2 domains neighboring them. Inside the hybrid ribbons,

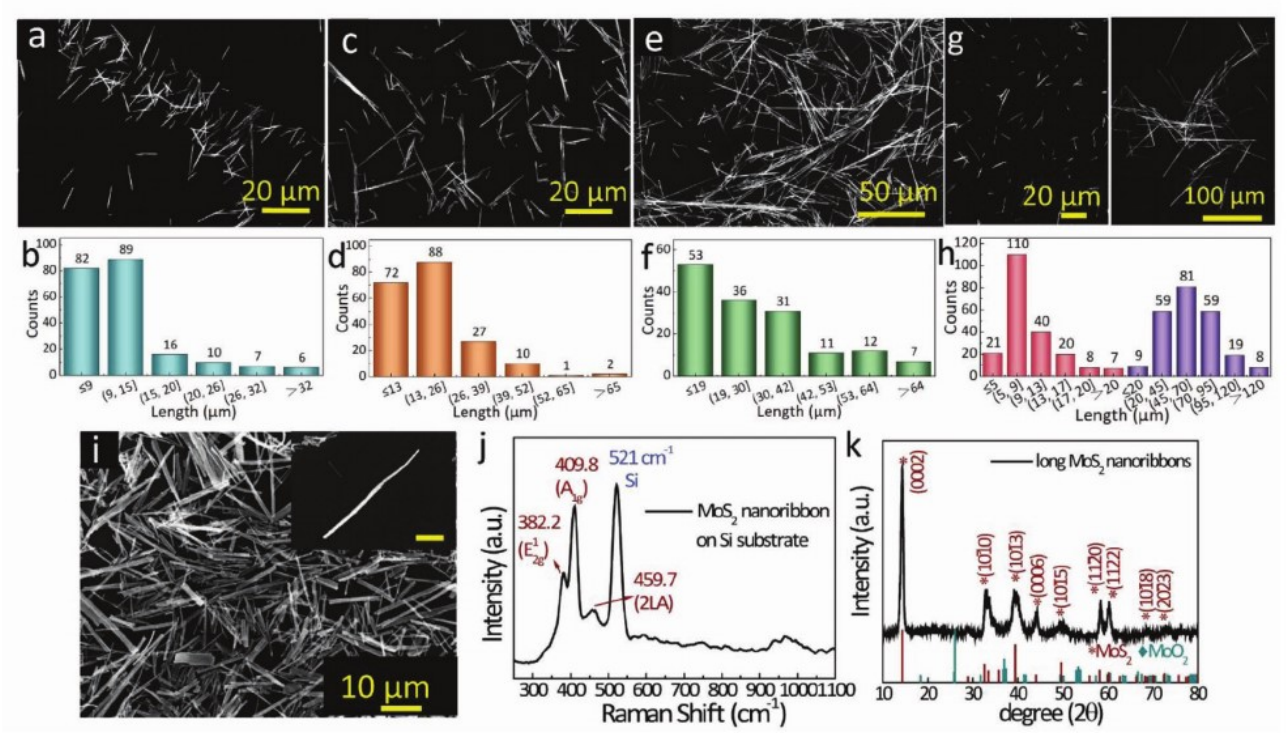

Figure 2. Tuning the dimensions of MoS_2 nanoribbons by adjusting the acidity of the precursor solution. a–d) SEM images and the length distribution of: a,b) MoO_3 nanoribbons synthesized with at pH = 0.0 (3.24×10^{-3} M $(NH_4)_6Mo_7O_{24}{\cdot}4H_2O$ and 0.573 M HNO_3); c,d) pH = –0.32 (3.24×10^{-3} M $(NH_4)_6Mo_7O_{24}{\cdot}4H_2O$ and 1.15 M HNO_3); and e,f) pH = –1.0 (3.24×10^{-3} M $(NH_4)_6Mo_7O_{24}{\cdot}4H_2O$ and 2.87 M HNO_3). a,c,e) SEM images show the general morphology of MoO_3 nanoribbon. Multiple SEM images with higher magnification are used to characterize the length distribution in (b,d,f). The length distribution of the MoO_3 nanoribbons synthesized at pH = –1.0 can be further refined by a 40 μm pore size filtration paper. g) SEM image and h) length distribution of refined long and short MoO_3 nanoribbons. i) MoS_2 nanoribbons of tens of micrometers can be obtained with j,k) the corresponding Raman spectrum (j) and XRD spectrum (k), scale bar of inset: 10 μm.

the (0002) MoS_2 planes also appear amidst the ($\bar{1}02$) MoO_2 domains. A gradual lattice transition can be observed in the TEM image (Figure S8, Supporting Information). Across the entire length of the nanoribbons, MoS_2 and MoO_2 form largely alternating lamellar structures as shown in the high-angle annular dark-field (HAADF) scanning transmission electron microscopy (STEM) images and electron energy loss spectroscopy (EELS) mapping (Figure 3c–g). Correlated analysis indicates that the MoO_2 and MoS_2 are in the bright and grey areas in HAADF-STEM images, respectively. The MoO_2 forms a continuous network, while MoS_2 covers the surface and is distributed in long island structures inside the hybrid ribbon. Owing to its unique structure, metallic MoO_2 could play an essential role in the electric conductivity of the hybrid ribbons. Our further characterization of the structure with energy-dispersive X-ray spectroscopy (EDS) supports the EELS analysis (Figure S9, Supporting Information).

After a second sulfurization at 900 °C, all the MoO_2 regions in the obtained MoS_2/MoO_2 hybrid nanoribbons convert into MoS_2 (Figure 3h,i). In addition to the aforediscussed Raman and XRD studies (Figure 1), the chemistry of the MoS_2 nanoribbons is further confirmed by phase-contrast TEM, EELS, and EDS mappings. No oxygen or its compound signal can be detected with the above techniques (Figure S10, Supporting Information). Moreover, the synthesized MoS_2 nanoribbons exhibit high thermal stability as shown by the TEM images in Figure 3j of in situ heated TEM samples. No morphological change can be observed from the MoS_2 nanoribbon even after the sample is subjected to a continuous heat treatment inside the TEM at 800 °C for 80 min, 900 °C for 20 min, and then 1000 °C for 20 min. This provides further evidence supporting the purity of the obtained MoS_2 nanoribbons, considering the melting temperature of bulk MoO_2 is only 1100 °C.

An advantage of the above growth procedure is not only that the nanoribbons can be obtained in large quantities, but that they can also be easily dispersed in a suspension. This is beneficial for applications of MoS_2 in solution. We can therefore demonstrate that it is possible to select, manipulate, and assemble nanoribbons at designated positions.

Here we utilize a versatile electric manipulation technique to orient and position individual MoS_2 nanoribbons in solution on a substrate.[26] Then upon UV light exposure, a chemical click-reaction fixes the nanoribbon on the substrate with high accuracy in the position and angle. This could for instance be helpful to assemble a MoS_2 device or to maneuver the nanostructures to pre-defined electrical contacts. Among the various nanomanipulation methods, which have made impressive contributions to the creation of artificial micro/nanoscale machines,[27] electric manipulation has demonstrated a high degree of control and precision, particularly for the manipulation of longitudinal nanoparticles.[26] More importantly, the technique can be applied to nanoparticles made of all materials,

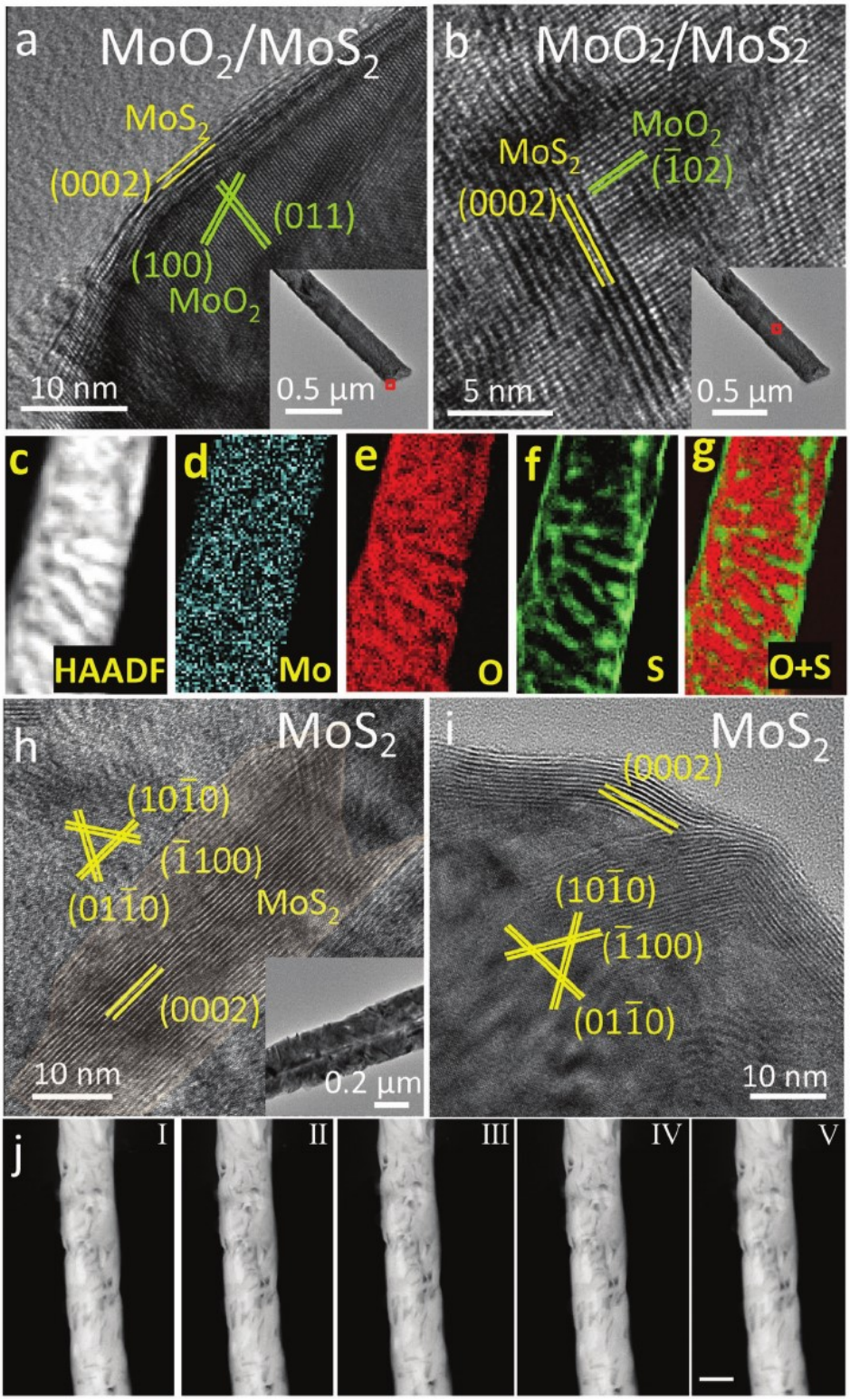

Figure 3. a,b) Phase-contrast TEM of the edge (a) and center (b) regions of MoS_2/MoO_2 hybrid nanoribbon. c) HAADF-STEM image of MoS_2/MoO_2 hybrid nanoribbon and d–g) the corresponding EELS mapping of elements Mo (d), O (e), S (f), and mixture of O and S (g), showing the distribution of MoS_2 in the hybrid ribbon. h,i) Phase-contrast TEM of the center (h) and edge (i) of MoS_2 nanoribbon. j) In situ HAADF-STEM image of MoS_2 nanoribbon at room temperature (I) and heated at 800 °C for 30 min (II), at 800 °C for 80 min (III), at 900 °C for 20 min (IV), and at 1000 °C for 20 min (V) continuously. No observable structural change can be found. Scale bar: 100 nm.

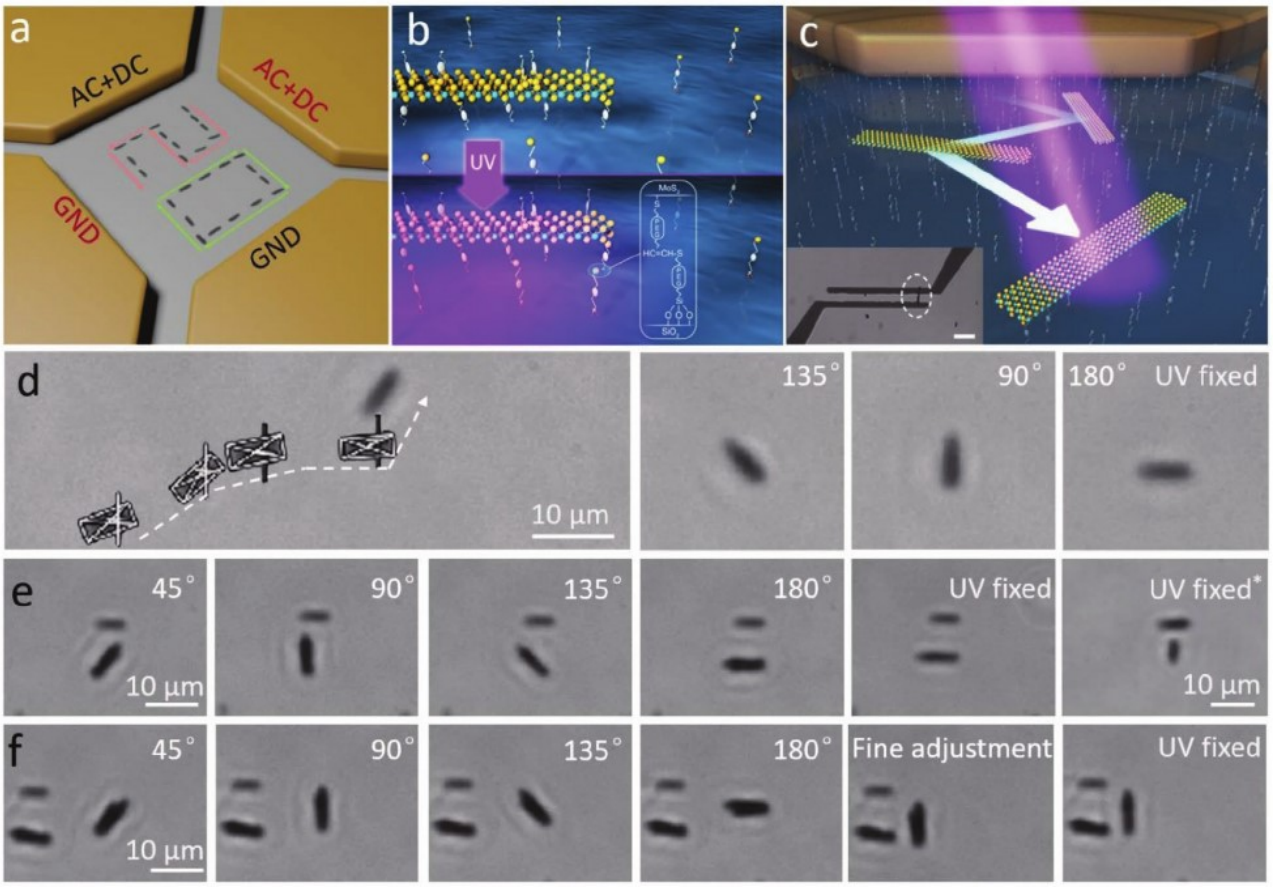

Figure 4. Assembly of MoS_2 nanoribbons with thiol-yne "click-chemistry" onto a substrate. a) Overlapped snapshots of a MoS_2 nanoribbon moving in a quadruple microelectrode along the prescribed trajectory to write "20." b) Top: Functionalization of MoS_2 nanoribbons and a glass substrate with thiol-PEG-alkyne and silane-PEG-thiol, respectively. Bottom: Immobilization of MoS_2 ribbons by UV-triggered thiol-yne click chemistry. c) Schematic shows the assembly process with controlled position and orientations before the chemical assembly. Inset: optical microscopy image of a MoS_2 nanoribbon directly assembled to a pair of prepatterned microelectrodes. Scale bar: 20 μm. d–f) Multiple MoS_2 nanoribbons assembled into different configurations after "click" chemical reaction.

including metals, semiconductors, and insulators, which suggests its suitability to manipulate MoS_2 nanostructures. The working principle of the electric manipulation has been described previously.[28] Briefly, uniform DC and AC electric fields are used in the manipulation. A longitudinal nanostructure, which naturally carries surface charges, can be moved in the direction of the DC field due to Coulomb interactions. The AC field can be used to exert a torque, which allows the angular orientation.[29,30] The transport and alignment are thus independently controlled. In the experiment, we disperse the MoS_2 nanoribbons at the center (500 μm × 500 μm) of a patterned quadrupole microelectrode as shown in **Figure 4**a. Applying the combined DC and AC electric fields with feedback control, the nanoribbons instantly move along the X and Y directions alternatively, tracing a designed 2D trajectory as shown in Movie S1, Supporting Information. Snapshots are overlapped and shown in Figure 4a. With this manipulation, a nanoribbon can be selected and transported to a designated position and aligned.

It is then possible to fix the position of nanoribbons. Since the MoS_2 nanoribbons are sulfur-rich with clear edges and grain boundaries, as shown by the TEM results in Figure 3h, many unsaturated sulfur sites are available to react with molecular thiol groups.[31] For this we exploit a light-triggered thiol-yne click-reaction to covalently fix the nanoribbon once it reaches a designated position.[32] The scheme of the thiol-yne click chemistry is implemented by conjugating the MoS_2 nanoribbons with the thiol groups of thiol-PEG-alkyne molecules, leaving the active alkyne groups on the outer surface, and terminating the surface of a glass substrate with thiol groups by conjugating with silane-PEG-thiol molecules (as illustrated in Figure 4b, details in Supporting Information). When a functionalized MoS_2 nanoribbon has been directed to a designated position, a short exposure with UV light, initiates the "click" reaction between the thiol and the alkyne groups (Figure 4c). The assembly of a MoS_2 nanoribbon occurs in 5–10 s "at the press of a light button". The reaction and assembly process is well reproducible. We have demonstrated the transport, orientation, and positioning of multiple MoS_2 nanoribbons next to each other into various patterns (Figure 4d–f and Movie S2, Supporting Information). With this technique, the MoS_2 nanoribbons also can be directly assembled to a pair of prepatterned microelectrodes (inset of Figure 4c and Movie S3, Supporting

Information). The precision in position and orientation is determined as 144 ± 601 and 111 ± 268 nm for the *X*, *Y* position and −1.85 ± 3.21° for the angle, respectively. The polycrystalline nature of the synthesized MoS_2 nanoribbons contributes to the robust and rapid assembly, because it is expected to show more reactive sulfur defects compared to the single-crystalline counterparts. To support this analysis, control experiments are carried by testing the assembly of functionalized Au–SiO_2 core–shell nanowires (counterpart of glass) on single-crystal MoS_2 nanoflakes (counterpart of our polycrystalline MoS_2). As shown in Movie S4, Supporting Information, functionalized Au-SiO_2 core–shell nanowires cannot fix on to the MoS_2 nanoflakes even after a continuous 40 s UV exposure. However, all the functionalized MoS_2 nanoribbons can quickly assemble on glass in around 10 s of UV illumination (Movie S5, Supporting Information). In these experiments, the conditions are controlled to be the same. We expect this assembly strategy could also be useful for assembling devices and for other TMD materials.

An important first step toward obtaining functional nanodevices is to reproducibly fabricate nanostructures with controlled composition, dimension, and chemistry.[33] Due to the layered crystal structure, it is challenging to synthesize 2D TMD materials with dimensional control, particularly into a longitudinal structure. We herein present a robust and scalable approach to synthesize MoS_2 nanoribbons with tunable dimensions and demonstrate their transfer, manipulation, and assembly "at the press of a light button." Compared to previous report,[7] the obtained MoS_2 nanoribbons are not adherent, and thus can be readily collected after growth. They can be dispersed in water where they can be moved along defined trajectories—positioned, oriented, and assembled in 2D patterns. The MoS_2 nanoribbons are rich in reactive sulfur sites which are an enabling factor in their chemical functionalization and the subsequent rapid assembly to a substrate with a light-triggered "click" reaction. Overall, the fabrication and assembly of MoS_2 nanoribbons demonstrated in our work might provide a new pathway to alleviate the roadblocks of applications of 2D materials. For instance, as demonstrated earlier, the MoS_2 nanoribbon can be directly assembled to a pair of prepatterned electrodes with controlled position and alignment (Figure 4 and Movie S3, Supporting Information). However, every coin has two sides. Compared to those single-crystalline MoS_2 structures made by exfoliated flakes and the recently reported MoS_2 nanostructures obtained by substrate assisted fabrication,[7] our MoS_2 nanoribbons exhibit polycrystalline features. For applications in electronic devices, this may not be ideal as a controlled number of layers in single-crystal MoS_2 can be used to tune its bandgap. The low defect density of a few-layer single-crystal structure also provides enhanced performance for optoelectronics.[8] However, the intrinsic semiconductor properties of MoS_2 can still be exploited for the utilization relevant to electronics, particularly given the merit of low-cost, scalable, and dimension-controlled synthesis. Here we study the optoelectronic performance of the fabricated MoS_2 nanoribbons on SiO_2/Si substrates to demonstrate its potential as photodetectors. As shown in **Figure 5**, the device shows a fast response to light with a wavelength from 450 to 750 nm, the performance of which is similar to that of single-crystal MoS_2 but at a lower increase in magnitude.[34]

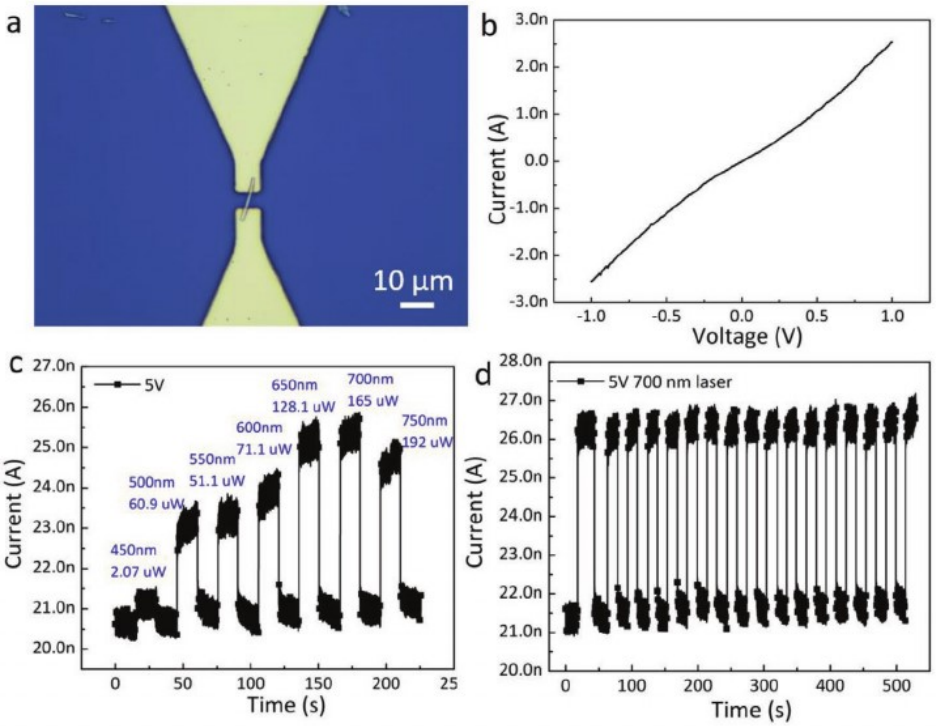

Figure 5. Optoelectronic performance of the MoS_2 nanoribbons. a) Optical microscopy image and b) *I*–*V* curve of the MoS_2 device fabricated on a SiO_2/Si substrate. c) Photoresponse of the MoS_2 nanoribbon with a bias voltage of 5 V to light with wavelengths from 450 to 750 nm. d) Rapid photoresponse of the MoS_2 nanoribbon under 700 nm laser illumination. The rise time and decay time are ≈8 and 16 ms, respectively.

Moreover, a large array of theoretical and experimental research points out that MoS_2 exhibits excellent catalytic activities and is much cheaper than catalysts formed from precious metals. This is attributed to the edges and points to the defects in MoS_2 nanostructures.[35] For a similar reason, the as-obtained MoS_2 nanoribbons demonstrate effective removal of mercury for water purification (Figure S11, Supporting Information). Overall, the structural tunable fabrication of MoS_2 nanoribbons with high yield and dispersibility, low-cost, as well as their light-triggered precision assembly may inspire the future fabrication and assembly of 2D TMD materials in various applications. Owing to the attributes of semiconductor and polycrystalline nature, the MoS_2 materials also show useful properties for optoelectronics and water purification.

Experimental Section

The details of the materials synthesis, functionalization and assembly process can be found in the Supporting Information.

The morphology of the ribbons synthesized at different stages were characterized using a scanning electron microscope (SEM, Hitachi S-5500) in a secondary electron scattering mode at 20 kV and a JEOL 2010 TEM operated at 200 kV. The composition of the samples was characterized by XRD (Rigaku MiniFlex 600), Raman spectrum (Alpha 300, excited by 475 nm laser), as well as EELS and EDS mapping in a double-corrected TEM/STEM FEI Titan G3 Cubed Themis at the International Iberian Nanotechnology Laboratory, Braga, Portugal.

Supporting Information

Supporting Information is available from the Wiley Online Library or from the author.

Acknowledgements

The authors thank the support by the Welch Foundation (F-1734), National Science Foundation (CMMI- 1563382, EECS-1710922, and EECS-1930649). D.F. and Y.H. thank the travel support from the UT Austin-Portugal program. This work was also supported by FCT, through IDMEC, under LAETA, project UIDB/50022/2020.

Conflict of Interest

The authors declare no conflict of interest.

Keywords

assembly, click chemistry, manipulation, MoS_2, transition metal dichalcogenides

Received: May 19, 2020
Revised: July 30, 2020
Published online: September 21, 2020

[1] a) S. Z. Butler, S. M. Hollen, L. Cao, Y. Cui, J. A. Gupta, H. R. Gutiérrez, T. F. Heinz, S. S. Hong, J. Huang, A. F. Ismach, *ACS Nano* **2013**, *7*, 2898; b) X. Huang, Z. Zeng, H. Zhang, *Chem. Soc. Rev.* **2013**, *42*, 1934; c) K. F. Mak, J. Shan, *Nat. Photonics* **2016**, *10*, 216.

[2] a) T. F. Jaramillo, K. P. Jørgensen, J. Bonde, J. H. Nielsen, S. Horch, I. Chorkendorff, *Science* **2007**, *317*, 100; b) A. M. Appel, D. L. DuBois, M. Rakowski DuBois, *J. Am. Chem. Soc.* **2005**, *127*, 12717; c) D. Voiry, M. Salehi, R. Silva, T. Fujita, M. Chen, T. Asefa, V. B. Shenoy, G. Eda, M. Chhowalla, *Nano Lett.* **2013**, *13*, 6222; d) G. Li, Z. Chen, Y. Li, D. Zhang, W. Yang, Y. Liu, L. Cao, *ACS Nano* **2020**, *14*, 1707.

[3] a) K. Kalantar-zadeh, J. Z. Ou, T. Daeneke, M. S. Strano, M. Pumera, S. L. Gras, *Adv. Funct. Mater.* **2015**, *25*, 5086; b) K. Kalantar-zadeh, J. Z. Ou, *ACS Sens.* **2016**, *1*, 5; c) S.-K. Li, Z.-T. Liu, J.-Y. Li, A.-Y. Chen, Y.-Q. Chai, R. Yuan, Y. Zhuo, *ACS Appl. Mater. Interfaces* **2018**, *10*, 14483.

[4] a) B. Radisavljevic, A. Radenovic, J. Brivio, V. Giacometti, A. Kis, *Nat. Nanotechnol.* **2011**, *6*, 147; b) S. B. Desai, S. R. Madhvapathy, A. B. Sachid, J. P. Llinas, Q. Wang, G. H. Ahn, G. Pitner, M. J. Kim, J. Bokor, C. Hu, H.-S. P. Wong, A. Javey, *Science* **2016**, *354*, 99.

[5] W. Li, M. C. Tekell, Y. Huang, K. Bertelsmann, M. Lau, D. Fan, *Adv. Energy Mater.* **2018**, *8*, 1802108.

[6] K. F. Mak, C. Lee, J. Hone, J. Shan, T. F. Heinz, *Phys. Rev. Lett.* **2010**, *105*, 136805.

[7] T. Chowdhury, J. Kim, E. C. Sadler, C. Li, S. W. Lee, K. Jo, W. Xu, D. H. Gracias, N. V. Drichko, D. Jariwala, T. H. Brintlinger, T. Mueller, H.-G. Park, T. J. Kempa, *Nat. Nanotechnol.* **2020**, *15*, 29.

[8] Q. H. Wang, K. Kalantar-zadeh, A. Kis, J. N. Coleman, M. S. Strano, *Nat. Nanotechnol.* **2012**, *7*, 699.

[9] M. A. R. Anjum, H. Y. Jeong, M. H. Lee, H. S. Shin, J. S. Lee, *Adv. Mater.* **2018**, *30*, 1707105.

[10] J. Wang, J. Liu, D. Chao, J. Yan, J. Lin, Z. X. Shen, *Adv. Mater.* **2014**, *26*, 7162.

[11] C. Liu, D. Kong, P. C. Hsu, H. Yuan, H. W. Lee, Y. Liu, H. Wang, S. Wang, K. Yan, D. Lin, *Nat. Nanotechnol.* **2016**, *11*, 1098.

[12] S.-Y. Cho, S. J. Kim, Y. Lee, J.-S. Kim, W.-B. Jung, H.-W. Yoo, J. Kim, H.-T. Jung, *ACS Nano* **2015**, *9*, 9314.

[13] a) A. K. Singh, P. Kumar, D. Late, A. Kumar, S. Patel, J. Singh, *Appl. Mater. Today* **2018**, *13*, 242; b) Q. Yun, Q. Lu, X. Zhang, C. Tan, H. Zhang, *Angew. Chem., Int. Ed.* **2018**, *57*, 626; c) S. Najmaei, Z. Liu, W. Zhou, X. Zou, G. Shi, S. Lei, B. I. Yakobson, J.-C. Idrobo, P. M. Ajayan, J. Lou, *Nat. Mater.* **2013**, *12*, 754; d) W. Li, Y. Huang, Y. Liu, M. C. Tekell, D. E. Fan, *Nano Today* **2019**, *29*, 100799.

[14] M. Remskar, A. Mrzel, Z. Skraba, A. Jesih, M. Ceh, J. Demšar, P. Stadelmann, F. Lévy, D. Mihailovic, *Science* **2001**, *292*, 479.

[15] J. Chen, N. Kuriyama, H. Yuan, H. T. Takeshita, T. Sakai, *J. Am. Chem. Soc.* **2001**, *123*, 11813.

[16] a) X. L. Li, Y. D. Li, *Chem. - Eur. J.* **2003**, *9*, 2726; b) Z. Chen, D. Cummins, B. N. Reinecke, E. Clark, M. K. Sunkara, T. F. Jaramillo, *Nano Lett.* **2011**, *11*, 4168.

[17] a) D. Akinwande, C. Huyghebaert, C.-H. Wang, M. I. Serna, S. Goossens, L.-J. Li, H. S. P. Wong, F. H. L. Koppens, *Nature* **2019**, *573*, 507; b) E. Singh, P. Singh, K. S. Kim, G. Y. Yeom, H. S. Nalwa, *ACS Appl. Mater. Interfaces* **2019**, *11*, 11061; c) J. Cheng, C. Wang, X. Zou, L. Liao, *Adv. Opt. Mater.* **2019**, *7*, 1800441.

[18] L. Chen, M. Zhang, X. Yang, W. Li, J. Zheng, W. Gan, J. Xu, *J. Alloys Compd.* **2017**, *695*, 3339.

[19] Molybdenum trioxide, https://pubchem.ncbi.nlm.nih.gov/compound/Molybdenum-trioxide (accessed: May 2020).

[20] X.-L. Li, J.-F. Liu, Y.-D. Li, *Appl. Phys. Lett.* **2002**, *81*, 4832.

[21] ITWG Guideline on Powder X-ray Diffraction (XRD)—general overview, http://www.nf-itwg.org/pdfs/ITWG-INFL-PXRD.pdf (accessed: May 2020).

[22] a) B. C. Windom, W. Sawyer, D. W. Hahn, *Tribol. Lett.* **2011**, *42*, 301; b) Y. Jin, P. K. Shen, *J. Mater. Chem. A* **2015**, *3*, 20080; c) D. Kong, H. Wang, J. J. Cha, M. Pasta, K. J. Koski, J. Yao, Y. Cui, *Nano Lett.* **2013**, *13*, 1341.

[23] J. Rajeswari, P. S. Kishore, B. Viswanathan, *Electrochem. Commun.* **2009**, *11*, 572.

[24] Y. Shi, B. Guo, S. A. Corr, Q. Shi, Y. S. Hu, K. R. Heier, L. Chen, R. Seshadri, G. D. Stucky, *Nano Lett.* **2009**, *9*, 4215.
[25] Y. Jin, H. Wang, J. Li, X. Yue, Y. Han, P. K. Shen, Y. Cui, *Adv. Mater.* **2016**, *28*, 3785.
[26] K. Kim, X. Xu, J. Guo, D. L. Fan, *Nat. Commun.* **2014**, *5*, 3632;
[27] a) G.-Z. Yang, J. Bellingham, P. E. Dupont, P. Fischer, L. Floridi, R. Full, N. Jacobstein, V. Kumar, M. McNutt, R. Merrifield, *Sci. Rob.* **2018**, *3*, eaar7650; b) S. Palagi, P. Fischer, *Nat. Rev. Mater.* **2018**, *3*, 113; c) K. Kim, J. Guo, Z. Liang, D. Fan, *Adv. Funct. Mater.* **2018**, *28*, 1705867; d) W. Wang, W. Duan, S. Ahmed, T. E. Mallouk, A. Sen, *Nano Today* **2013**, *8*, 531.
[28] D. Fan, Z. Yin, R. Cheong, F. Q. Zhu, R. C. Cammarata, C. L. Chien, A. Levchenko, *Nat. Nanotechnol.* **2010**, *5*, 545.
[29] D. Fan, R. Cammarata, C. L. Chien, *Appl. Phys. Lett.* **2008**, *92*, 1316.
[30] Z. Liang, D. Teal, D. Fan, *Nat. Commun.* **2019**, *10*, 5275.
[31] S. S. Chou, M. De, J. Kim, S. Byun, C. Dykstra, J. Yu, J. Huang, V. P. Dravid, *J. Am. Chem. Soc.* **2013**, *135*, 4584.
[32] D. Walker, D. P. Singh, P. Fischer, *Adv. Mater.* **2016**, *28*, 9846.
[33] A. G. Mark, J. G. Gibbs, T.-C. Lee, P. Fischer, *Nat. Mater.* **2013**, *12*, 802.
[34] a) Z. Yin, H. Li, H. Li, L. Jiang, Y. Shi, Y. Sun, G. Lu, Q. Zhang, X. Chen, H. Zhang, *ACS Nano* **2012**, *6*, 74; b) H. S. Lee, S.-W. Min, Y.-G. Chang, M. K. Park, T. Nam, H. Kim, J. H. Kim, S. Ryu, S. Im, *Nano Lett.* **2012**, *12*, 3695.
[35] J. Xie, H. Zhang, S. Li, R. Wang, X. Sun, M. Zhou, J. Zhou, X. W. Lou, Y. Xie, *Adv. Mater.* **2013**, *25*, 5807.